Nanoporous $Ni(OH)_2$ Thin Film on 3D Ultrathin-Graphite Foam for Asymmetric Supercapacitor

Junyi Ji,[†,‡] Li Li Zhang,[†,*] Hengxing Ji,[†] Yang Li,[‡] Xin Zhao,[†] Xin Bai,[†] Xiaobin Fan,[‡] Fengbao Zhang,[‡] and Rodney S. Ruoff[†,*]

[†]Department of Mechanical Engineering and the Materials Science and Engineering Program, The University of Texas at Austin, 1 University Station C2200, Austin, Texas 78712, United States and [‡]School of Chemical Engineering & Technology, Tianjin University, Tianjin 300072, China

ABSTRACT Nanoporous nickel hydroxide ($Ni(OH)_2$) thin film was grown on the surface of ultrathin-graphite foam (UGF) *via* a hydrothermal reaction. The resulting free-standing $Ni(OH)_2$/UGF composite was used as the electrode in a supercapacitor without the need for addition of either binder or metal-based current collector. The highly conductive 3D UGF network facilitates electron transport and the porous $Ni(OH)_2$ thin film structure shortens ion diffusion paths and facilitates the rapid migration of electrolyte ions. An asymmetric supercapacitor was also made and studied with $Ni(OH)_2$/UGF as the positive electrode and activated microwave exfoliated graphite oxide ('a-MEGO') as the negative electrode. The highest power density of the fully packaged asymmetric cell (44.0 kW/kg) was much higher (2—27 times higher), while the energy density was comparable to or higher, than high-end commercially available supercapacitors. This asymmetric supercapacitor had a capacitance retention of 63.2% after 10 000 cycles.

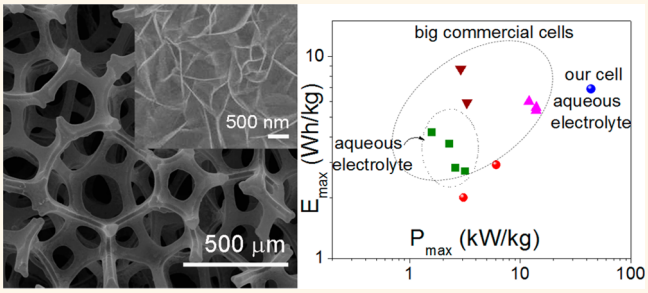

KEYWORDS: $Ni(OH)_2$ · ultrathin-graphite foam · composite · supercapacitor · asymmetric

Supercapacitors (also known as electrochemical capacitors or ultracapacitors) with high power density and long lifespan are of interest as energy storage devices.[1−4] Pseudocapacitors, utilizing in principle fast and reversible electrochemical redox reactions from materials such as RuO_2,[5,6] MnO_2,[7,8] NiO,[9] Co_3O_4,[10] and $Ni(OH)_2$,[11,12] often have very high theoretical capacitance. However, they usually suffer from poor stability, low conductivity and large volume change during the charge/discharge processes.[1] Among various 'pseudoactive' materials, nickel hydroxide ($Ni(OH)_2$) is cost-effective and is available in various morphologies, making it an attractive candidate for high performance supercapacitors. In attempts to improve the electrochemical performance of $Ni(OH)_2$-based electrodes, $Ni(OH)_2$ nanostructures have been studied,[13,14] as well as $Ni(OH)_2$-carbon composites involving high-surface-area conductive materials such as carbon nanotubes,[15,16] activated carbon[17,18] and graphene.[12,19−21] These materials can improve the conductivity of the composites and shorten the electron and ion diffusion pathways with the aim of more efficient charge and mass exchange. Such nanostructured composites have always been coated to a metal current collector to obtain a continuous conductive structure, which greatly decreases the overall gravimetric specific capacitance. The typical addition of a polymeric binder will not only hamper the charge transport rate, but also further increase the total mass of the electrode. Recently, three-dimensional (3D) nickel foam was used as a substrate to grow $Ni(OH)_2$ thin film to exploit the conductive backbone of the nickel foam,[22−25] and the resulting 3D porous structures showed improved capacitance without the addition of a binder. However, considering the weight of the nickel foam (density of about 262 mg/cm^3, thickness of 1.6 mm), the gravimetric capacitance with respect to the total mass of the electrode has been very low (12−38 F/g, $Ni(OH)_2$ loading density on nickel foam has always been less than 1 mg/cm^2).[22,23,25]

* Address correspondence to r.ruoff@mail.utexas.edu, g0600003@gmail.com.

Received for review May 1, 2013 and accepted June 11, 2013.

Published online June 11, 2013
10.1021/nn4021955

Ultrathin-graphite foam (UGF),[26] a foam structure consisting of ultrathin graphite struts reported in our previous work,[27] provides a low density (10−20 mg/cm^3) free-standing 3D interconnected network with high electrical conductivity (~1.3 × 10^5 S/m at 300 K).[27] These properties make UGF a promising candidate to replace traditional current collectors such as nickel foam or carbon paper. We report a binder-free $Ni(OH)_2$/UGF composite by direct growth of a porous $Ni(OH)_2$ thin film on the UGF surface by hydrothermal reaction. The interconnected 3D conductive network of the UGF ensures a high electron conductivity and the porous structure of the $Ni(OH)_2$ film offers a short ion diffusion pathway. The $Ni(OH)_2$/UGF composite had a specific capacitance of 166 and 111 F/g at current densities of 0.5 and 10 A/g, respectively, based on the total mass of the electrode including the UGF current collector. (Based on the mass of $Ni(OH)_2$, the specific capacitance values are (1.56 ± 0.06) × 10^3 and (1.04 ± 0.04) × 10^3 F/g, respectively.)

An aqueous electrolyte (environmentally benign) based asymmetric supercapacitor using $Ni(OH)_2$/UGF composite as the positive electrode and activated microwave exfoliated graphite oxide ('a-MEGO') as the negative electrode has demonstrated high power density and moderately high energy density in a fully packaged supercapacitor cell at an operating potential of 1.8 V.

RESULTS AND DISCUSSIONS

The structure of the $Ni(OH)_2$/UGF composite was studied by X-ray diffraction (XRD, Figure 1a). All the diffraction peaks of the $Ni(OH)_2$/UGF composite are either due to graphite (they are identical to those of pure UGF) or to β-$Ni(OH)_2$ (JCPDS: 14-0117). The X-ray photoelectron spectroscopy (XPS) pattern of the $Ni(OH)_2$/UGF composite (Figure 1b) shows the binding energy of Ni $2p_{3/2}$ centered at 856.1 eV, typical of the Ni^{2+} phase of $Ni(OH)_2$. Based on separate TGA studies of the $Ni(OH)_2$ powder, the UGF, and the $Ni(OH)_2$/UGF composite (Figure S1; TGA done in the temperature range of 35−950 °C under air atmosphere at a heating rate of 5 °C/min), the mass ratio of $Ni(OH)_2$ in the $Ni(OH)_2$/UGF composite was estimated to be 10.6%.

The Scanning Electron Microscopy (SEM) image in Figure 2a shows that the 3D interconnected structure of the UGF remains unchanged after $Ni(OH)_2$ deposition (Figure S2, see Supporting Information for the pristine UGF). No collapse of the graphite struts or obstruction of the pores is observed, indicating the strong mechanical strength of the UGF and the uniform dispersion of the $Ni(OH)_2$ film. The cross-sectional view shows that the $Ni(OH)_2$ film, with a thickness of ~2 μm, is well adhered to the UGF surface (Figure 2b). No peeling off of the $Ni(OH)_2$ film from the UGF surface was observed after vigorously shaking the composite in a glass bottle. The $Ni(OH)_2$ thin film

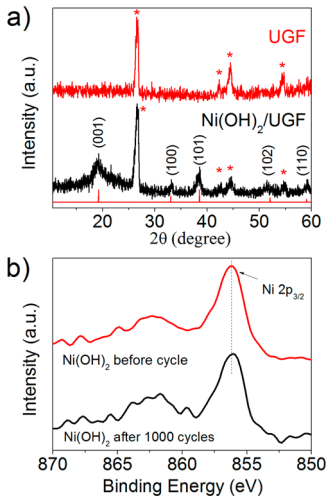

Figure 1. (a) The XRD patterns of the $Ni(OH)_2$/UGF composite and of UGF alone. (b) XPS spectra acquired from the $Ni(OH)_2$/UGF composite, of the Ni $2p_{3/2}$ region before and after the electrochemical cycling test.

exhibits a highly random porous architecture, which is composed of nanoflakes with thickness of about 20−30 nm (Figure 2a, inset). Some $Ni(OH)_2$ particles were observed in the solution from the same reaction batch that were not attached to the UGF, and they, also composed of nanoflakes, were roughly spherical with a diameter of about 2 μm (Figure S3, see Supporting Information).

With the decomposition of urea, $Ni(OH)_2$ nuclei formed on the UGF surface as well as in the solution. The anisotropy of the $Ni(OH)_2$ crystals leads to the growth of 'nanoflakes'.[13,28] The pH value decreases during growth of the nanoflakes and Ostwald-ripening occurs,[29,30] as larger flakes grow and consume smaller ones.[31] The large flakes were found to aggregate, likely driven by a reduction in total surface energy. Thus, nucleation on the UGF surface leads to the formation of a porous $Ni(OH)_2$ thin film, while nucleation in solution leads to spherical particles to minimize surface energy.[13,28,31−33] The structure of the $Ni(OH)_2$/UGF composite was also studied by EDS mapping (Figure 2c−f). The elemental maps of O and Ni showed a uniform and continuous dispersion throughout the UGF network, indicating a continuous $Ni(OH)_2$ film was formed on the UGF surface.

The $Ni(OH)_2$/UGF composite was considered for study as the electrode material for a supercapacitor because: (i) the 3D UGF provides a highly conductive network to enhance the electron transport to the $Ni(OH)_2$ film, (ii) the porous $Ni(OH)_2$ structure shortens ion diffusion paths and facilitates migration of electrolyte ions at large current density, and (iii) the free-standing structure avoids the addition of binder and a metal-based current collector which not only eliminates the additional contact resistance between the current collector and the active material, but also reduces the total mass of the electrode.

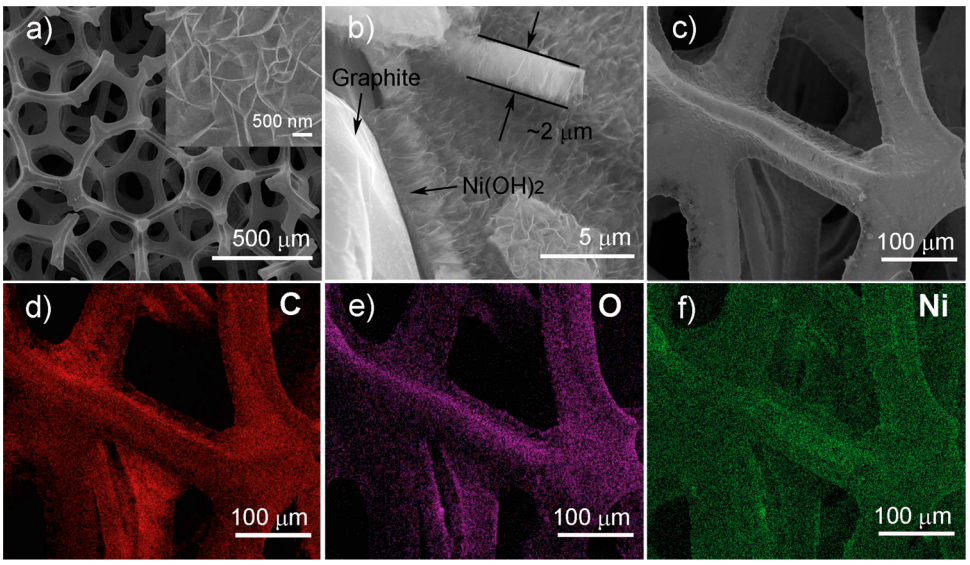

Figure 2. SEM images of the $Ni(OH)_2$/UGF composite, (a) SEM image of the composite material, and the inset shows a higher magnification image of the $Ni(OH)_2$ nanoflakes; (b) a cross-sectional view of the composite; (c) SEM image and the corresponding EDS elemental mapping images of (d) carbon, (e) oxygen, and (f) nickel.

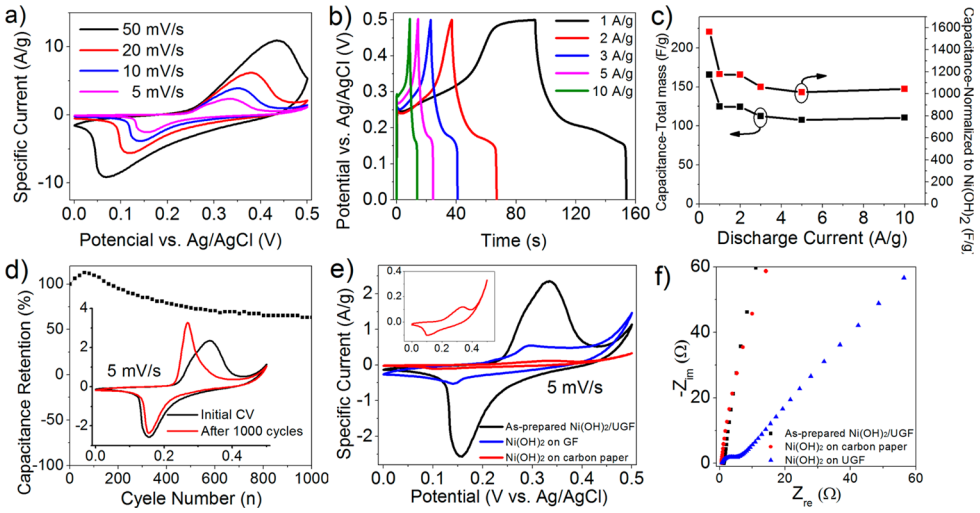

Figure 3. Three-electrode electrochemical measurements of the $Ni(OH)_2$/UGF composite in 6 M KOH aqueous solution. (a) CV curves at different scan rates; (b) galvanostatic charge−discharge curves at various current densities; (c) gravimetric specific capacitance of $Ni(OH)_2$/UGF composite as a function of the current densities, (d) cycling performance of $Ni(OH)_2$/UGF composite at 10 A/g, inset shows the CV curves before and after cycling at 5 mV/s, respectively; (e) CV curves (at 5 mV/s, inset is the magnifying CV curve of $Ni(OH)_2$ on carbon paper); (f) Nyquist plots of the as-prepared $Ni(OH)_2$/UGF composite, and of the $Ni(OH)_2$ nanoparticles slurry after drop-casting on UGF or carbon paper.

The electrochemical properties of the $Ni(OH)_2$/UGF composite were first evaluated using a three-electrode system in 6 M KOH aqueous solution. Figure 3a shows the CV curves of $Ni(OH)_2$/UGF composite at various scan rates in the potential range of 0−0.5 V *vs* Ag/AgCl. A pair of oxidation and reduction peaks can be seen, which are due to the reversible reaction of $Ni(OH)_2 + OH^- \leftrightarrow NiOOH + H_2O + e^-$.[34,35] The Coulombic efficiency obtained from the CV curve at the scan rate of 50 mV/s is 99.7%. The high Coulombic efficiency indicated fully reversible pseudocapacitive behavior of the $Ni(OH)_2$/UGF composite electrode. With increasing scan rate, the current increased and the oxidation peaks shifted to a more positive position and the reduction peaks to a more negative position. This is due to an increase of the internal diffusion resistance within the pseudoactive material with an increase in scan rate.[33,36] The gravimetric capacitance of the $Ni(OH)_2$/UGF electrode at various current densities was calculated from the discharge curves and is shown in Figure 3c. A gravimetric capacitance based on the total mass of the electrode (*i.e.*, UGF + $Ni(OH)_2$) was 166 F/g at a current density of 0.5 A/g (the current density was normalized based on the total mass of the electrode). The gravimetric capacitance can reach (1.56 ± 0.06) × 10^3 F/g based on the mass of $Ni(OH)_2$ alone at the same

current. When the current density was increased from 0.5 to 10 A/g, the gravimetric capacitance (based on the total mass of the electrode) decreased about 30% and then remained approximately constant at 111 A/g, implying good ion diffusion and electron transport ability at high current density. This rate performance highlights advantages of the nanoporous $Ni(OH)_2$/UGF composite, which provides fast and efficient diffusion of the electrolyte ions to the active material surface and excellent electron transport within the UGF struts.

(In our experiments, the $Ni(OH)_2$/UGF composite was typically 'crushed' in a roller and in this way the volume was significantly decreased. Rather than using a roller, in a control experiment a press was used and 15 MPa force applied. The $Ni(OH)_2$/UGF electrode then had a thickness of about 37 ± 3 μm; thus, the volumetric capacitance of the total electrode including the current collector was estimated to be about 93.5 ± 8 F cm^{-3}, comparable to that of EDL capacitors.[37,38])

The stability of the $Ni(OH)_2$/UGF composite was evaluated using a long-term galvanostatic charge/discharge process (Figure 3d). The capacitance increased during the first 100 cycles, which may be attributed to the activation of $Ni(OH)_2$ that allows trapped ions (ions can be trapped between the $Ni(OH)_2$ crystalline layers during the growth of nanoflakes) to diffuse out.[28,31] The capacitance stabilized in the last 400 cycles and a capacitance retention of about 65% was achieved after 1000 cycles at a current density of 10 A/g.

The CV curves of the electrode before and after the cycling test recorded at a scan rate of 5 mV/s are shown in Figure 3d (inset). Two CV curves exhibit a similar profile with a pair of oxidation/reduction peaks, except that the redox peaks are better defined and the potential difference between the two redox peaks is smaller after the cycling process (0.18 and 0.11 V for the initial and final cycle, respectively). The potential difference ΔE_{OR} ($E_O - E_R$) between the oxidation potential and the reduction potential is a measure of the reversibility of the redox reaction and the relatively small values obtained here indicates better reversibility.[34,35] The morphology and the chemical composition of the electrode appear to be unchanged after the cycling test, see SEM images (Figure S4, see Supporting Information) and XPS spectrum (Figure 1b). No deformation of the nanoflakes or peeling off from the UGF was observed, indicating a good stability of the porous $Ni(OH)_2$/UGF composite.

To reiterate, the relatively good capacitive performance of the 3D $Ni(OH)_2$/UGF composite is due to: (1) growth of the thin and porous active material onto the free-standing UGF which allows not using the poorly conductive and electrochemically nonactive binder; (2) the 3D interconnected structure provides a highly conductive network to effectively transfer sufficient electrons to the active material; (3) the larger surface area of the UGF (20 cm^2 per nominal area, which is ~20 times larger than that of a flat current collector), provides a more open surface for the contact of the active material which allows for a thinner active material layer under the same loading density; (4) the good contact between the active material and the UGF current collector facilitates electron transfer; and (5) the thin and porous $Ni(OH)_2$ nanoflakes within the 3D interconnected electrode structure ensures fast and efficient transport of the electrolyte ions.

To further test these suggested advantages of this 3D porous composite structure, two other electrodes were fabricated by direct drop-casting of $Ni(OH)_2$ particles on UGF and on carbon paper, respectively, with the same loading density of 0.2 mg/cm^2. Figure 3e shows the current response of the three types of electrodes at the scan rate of 5 mV/s. The specific current of the $Ni(OH)_2$/UGF electrode made as described above, based on the total mass of the electrode, is much higher than that for the other two, indicating better capacitive performance of this composite material.

The Nyquist plots of the three electrodes obtained using AC electrochemical impedance spectroscopy (EIS) in the frequency range from 100 kHz to 0.01 Hz are shown in Figure 3f and Figure S5 (see Supporting Information). The Nyquist plots of the $Ni(OH)_2$/UGF electrode have an almost vertical line in the low frequency region, indicating a good capacitive behavior. In the high frequency region, the $Ni(OH)_2$/UGF electrode and an equivalent series resistance (ESR) of about 1.3 Ω, suggesting a small electrode resistance and high charge-transfer rate between the electrolyte and the active material. In contrast, the other two electrodes prepared by the drop-casting method showed a large diffusion resistance in the high frequency region (about 5.2 and 510 Ω for $Ni(OH)_2$ on UGF and on carbon paper, respectively, see Figure 3f and Figure S5), indicating a poor charge-transfer rate.

An asymmetric supercapacitor was fabricated using $Ni(OH)_2$/UGF and a-MEGO[37,39] as the positive and negative electrode, respectively. One advantage of the asymmetric configuration is the use of the pseudocapacitive positive electrode to enhance the specific capacitance of the cell. On the other hand, the operating potential of the asymmetric cell can be extended due to the overpotential of reversible hydrogen electrosorption in a nanoporous carbon-based negative electrode.[15,20,21,40,41] A series of CV measurements with different voltage windows were used to estimate the best operating potential of the asymmetric supercapacitor cell (Figure 4a). When the operating potential window is 1.0 V, the presence of the redox peaks (in the region between 0.6 and 1.0 V) indicates the pseudocapacitive properties of the cell coming from the positive electrode ($Ni(OH)_2$/UGF). With an increase of the operating potential to 1.8 V, more faradic reactions (the larger current response) occurred. When the operating potential was extended to 2.0 V, evolution of oxygen occurred.[8] As both the energy density and

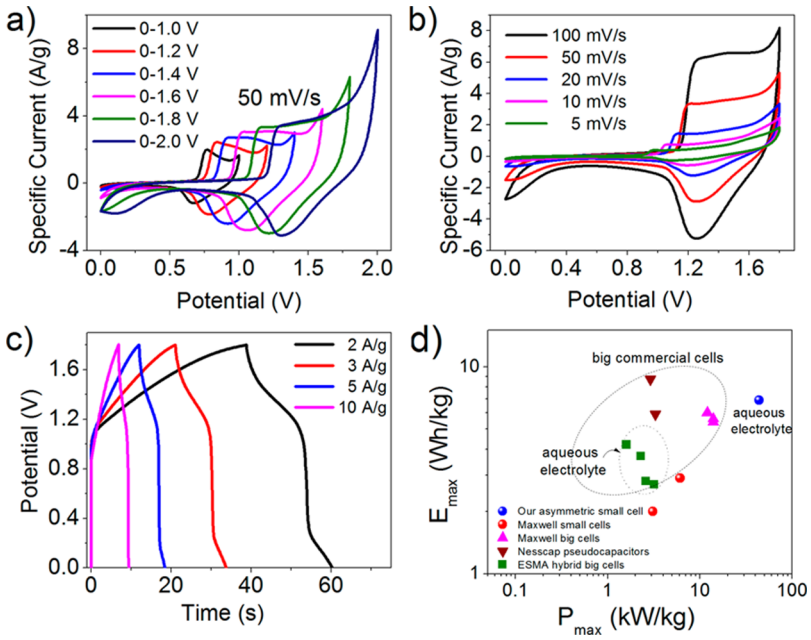

Figure 4. CV curves of $Ni(OH)_2$/UGF//a-MEGO asymmetric supercapacitor (a) measured at different potential window (at 50 mV/s) and (b) at different scan rates in 6 M KOH solution and (c) galvanostatic charge−discharge curves at different current densities; (d) Ragone plots of the asymmetric supercapacitor based on the full cell, comparing with some high-end commercial supercapacitors.

power density is highly dependent on the cell operating voltage according to $E = C_{single} \cdot V^2/8$, 1.8 V was used as the cell potential to further investigate the electrochemical performance of the asymmetric supercapacitor.

CV curves at different scan rates (ranging from 5 to 100 mV/s) were measured under 1.8 V in 6 M KOH (aq) solution (Figure 4b). A combination of both pseudocapacitive and EDL types of capacitance was clearly observed at all scan rates. The current increased with the scan rates, and the oxidation peak shifted to a more positive potential, similar to what was observed in the three-electrode configuration. The galvanostatic charge/discharge plots at different current densities with the potential window of 1.8 V are shown in Figure 4c. The specific capacitance calculated based on the total mass of the electrodes (total mass of both positive and negative electrodes) reached 119 F/g per electrode at a current density of 1 A/g. The capacitance retention of the asymmetric cell after 10 000 cycles of charge/discharge at a current density of 5 A/g is 63.2% (Figure S7, see Supporting Information), and indicates a relatively good stability of the asymmetric pseudocapacitor. The capacitance loss may be due to the loss of the electrical contact between the active materials ($Ni(OH)_2$) and the UGF because of change in volume of the active materials during cycling.

The energy densities and power densities of the asymmetric supercapacitor (based on the total mass of the electrodes, including the mass of UGF) are shown in Figure S6 (see Supporting Information). A maximum gravimetric energy density and power density of 13.4 Wh/kg and 85.0 kW/kg was obtained, respectively, based on the total weight of the electrodes including the UGF current collector in the asymmetric cell. The corresponding volumetric energy density and power density were estimated to be 8.7 Wh/L and 55.3 kW/L, respectively, based on the total electrode density of 0.65 g/cm^3 (Table S2, see Supporting Information for details of the calculation). In addition, the performance of the fully packaged asymmetric cell was also estimated (Table S2). With a weight ratio of 22% for the active electrode materials in a packaged device, a maximum practical gravimetric energy density of 6.9 Wh/kg (highest power density of 44.0 kW/kg) and volumetric energy density of 4.8 Wh/L (highest power density of 30.8 kW/L) was obtained for the packaged device. Table S3 (see Supporting Information) summarizes high-end commercial supercapacitor devices from various companies and a Ragone plot is shown in Figure 4d. The energy density of our hybrid supercapacitor is comparable or higher than most of the organic-based high-end supercapacitors, but the power density is much higher (2−27 times higher) than all the commercially available cells. Considering the use of environmentally benign aqueous electrolyte, our hybrid supercapacitor shows promise for application as a high power energy device.

CONCLUSION

In conclusion, a 3D interconnected $Ni(OH)_2$/UGF composite was made by growth of a porous $Ni(OH)_2$ thin film on the lightweight and highly conductive UGF surface. This $Ni(OH)_2$/UGF composite is free-standing and can be used as an electrode in a supercapacitor

without the addition of binder or use of a metal-based current collector, which dramatically decreases the total resistance as well as the total mass of the cell. An asymmetric supercapacitor based on $Ni(OH)_2$/UGF as the positive electrode and a-MEGO as the negative electrode in aqueous electrolyte had high power density with moderate energy density in a fully packaged cell. This simple and cost-effective synthetic method can be applied to other electroactive materials and offers promise for high power energy storage.

EXPERIMENTAL AND METHOD

Synthesis of $Ni(OH)_2$/UGF Composite. The ultrathin graphite foam (UGF) was synthesized by a chemical vapor deposition (CVD) method on a nickel foam used as a template as described in our previous report.[27] A pure graphite foam was achieved after etching the nickel away using a 3% HCl aqueous solution. The $Ni(OH)_2$/UGF composite was prepared by a hydrothermal reaction as follows: the UGF was placed in a filter flask. A total of 32 mg of $NiCl_2 \cdot 6H_2O$ and 50 mg of urea were added to 20 mL of DI water and this homogeneous solution was then added into the filter flask by an injector under vacuum to let the solution wet the UGF. After the UGF was totally wetted, all of the solution and the UGF were transferred into an autoclave reactor, which was heated to 180 °C for 2 h and then cooled to room temperature. The resulting $Ni(OH)_2$/UGF composite was then washed using DI water and then isopropyl alcohol several times, and dried in an air oven at 80 °C. A comparison sample was prepared by the same method without the addition of UGF, forming a $Ni(OH)_2$ powder after washing.

General Characterization. The $Ni(OH)_2$/UGF composite was characterized by X-ray diffraction (XRD, Xpert, Philips) using Cu K R radiation and X-ray photoelectron spectroscopy (XPS, PHI5000VersaProbe). Scanning electron microscopy (SEM, Quanta 600 FEG, FEI Company, 30 kV) equipped with energy-dispersive spectroscopy (Bruker EDS Quantax 4010) was used to study the morphology, microstructure, and elemental composition of the composites and related materials. Thermogravimetric analysis (TGA, Perkin-Elmer TGA 4000) was done using a 5 °C/min heating rate under 20 mL/min flow of air. All the materials were weighed by a high precision electronic balance (XP105DR, Mettler Toledo).

Electrochemical Characterization. A three-electrode system was used to measure the response of the $Ni(OH)_2$/UGF composite as the working electrode using 6 M KOH aqueous solution as the electrolyte, with a Pt mesh as the counter electrode and Ag/AgCl as the reference electrode, respectively. The powder sample used for the comparison samples was mixed with 5% poly(tetrafluoroethylene) (PTFE, Sigma-Aldrich, 60 wt % dispersion in water) in ethanol to form a homogeneous paste, then drop-casted separately onto the UGF and onto carbon paper.

The asymmetric supercapacitor was measured with a two-electrode system, where $Ni(OH)_2$/UGF composite was the positive electrode, and a-MEGO mixed with 5% PTFE to form a paste and then rolled into uniform sheet at a thickness of about 20 μm was the negative electrode. The two electrodes and a separator (Celgard 3501) permeable to ion transport were placed into a test fixture consisting of two stainless steel plates, with 6 M KOH aqueous solution as the electrolyte. All the electrochemical measurements were carried out with an Autolab (PGSTAT320N) electrochemical workstation. All the operating current densities were calculated based on the total mass of the system (whole electrode including the UGF current collector for the 3-electrode system and the total weight of the positive and negative electrodes including the UGF current collector for the 2-electrode system).

The gravimetric specific capacitance for the three-electrode cell was obtained from the galvanostatic charge/discharge curves as: $C_{single} = I \cdot t/m_s \cdot V$, where m_s (g) is the mass of the working electrode, I (A) is the current density, t (s) is the discharge time and V (V) is the discharge voltage range. For the two-electrode system, the mass ratio between the positive and negative electrode is obtained based on the following equation: $m_+/m_- = C_- \cdot V_-/C_+ \cdot V_+$, and the gravimetric specific capacitance is obtained by the equation: $C_{single} = 4I \cdot t/m \cdot V$, where m is the total mass of the two electrodes (including the mass of UGF). The energy density is calculated as: $E = C_{single} \cdot V_{max}^2/8$. The equivalent series resistance (ESR) is estimated by $R_{ESR} = V_{drop}/(2I)$, while the power density is calculated by the equation $P = V_{max}^2/(4mR_{ESR})$.

Conflict of Interest: The authors declare no competing financial interest.

Supporting Information Available: TGA curves, SEM images, Ragone plot, cycling performance of the asymmetric supercapacitor and comparison of the commercial high-end supercapacitors. This material is available free of charge *via* the Internet at http://pubs.acs.org.

Acknowledgment. We appreciate funding support from the U.S. Department of Energy (DOE) under award DE-SC0001951. J.J. is supported by the China Scholarship Council Fellowship.

REFERENCES AND NOTES

1. Wang, G.; Zhang, L.; Zhang, J. A Review of Electrode Materials for Electrochemical Supercapacitors. *Chem. Soc. Rev.* **2012**, *41*, 797–828.
2. Zhang, L. L.; Zhao, X. S. Carbon-Based Materials as Supercapacitor Electrodes. *Chem. Soc. Rev.* **2009**, *38*, 2520–2531.
3. Simon, P.; Gogotsi, Y. Materials for Electrochemical Capacitors. *Nat. Mater.* **2008**, *7*, 845–854.
4. Miller, J. R.; Simon, P. Electrochemical Capacitors for Energy Management. *Science* **2008**, *321*, 651–652.
5. Kim, H.; Popov, B. N. Characterization of Hydrous Ruthemium Oxide/Carbon Nanocomposite Supercapacitors Prepared by a Colloidal Method. *J. Power Sources* **2002**, *104*, 52–61.
6. Hu, C. C.; Chang, K. H.; Lin, M. C.; Wu, Y. T. Design and Tailoring of the Nanotubular Arrayed Architecture of Hydrous RuO_2 for Next Generation Supercapacitors. *Nano Lett.* **2006**, *6*, 2690–2695.
7. Chou, S.-L.; Wang, J.-Z.; Chew, S.-Y.; Liu, H.-K.; Dou, S.-X. Electrodeposition of MnO_2 Nanowires on Carbon Nanotube Paper as Free-Standing, Flexible Electrode for Supercapacitors. *Electrochem. Commun.* **2008**, *10*, 1724–1727.
8. Wu, Z. S.; Ren, W. C.; Wang, D. W.; Li, F.; Liu, B. L.; Cheng, H. M. High-Energy MnO_2 Nanowire/Graphene and Graphene Asymmetric Electrochemical Capacitors. *ACS Nano* **2010**, *4*, 5835–5842.
9. Lang, J.-W.; Kong, L.-B.; Wu, W.-J.; Luo, Y.-C.; Kang, L. Facile Approach To Prepare Loose-Packed NiO Nano-Flakes Materials for Supercapacitors. *Chem. Commun.* **2008**, *44*, 4213–4215.
10. Cao, L.; Lu, M.; Li, H.-L. Preparation of Mesoporous Nanocrystalline Co_3O_4 and Its Applicability of Porosity to the Formation of Electrochemical Capacitance. *J. Electrochem. Soc.* **2005**, *152*, A871–A875.
11. Lee, J. W.; Ahn, T.; Soundararajan, D.; Ko, J. M.; Kim, J.-D. Non-Aqueous Approach to the Preparation of Reduced Graphene Oxide/α-$Ni(OH)_2$ Hybrid Composites and Their High Capacitance Behavior. *Chem. Commun.* **2011**, *47*, 6305–6307.
12. Wang, H. L.; Casalongue, H. S.; Liang, Y. Y.; Dai, H. J. $Ni(OH)_2$ Nanoplates Grown on Graphene as Advanced Electrochemical Pseudocapacitor Materials. *J. Am. Chem. Soc.* **2010**, *132*, 7472–7477.
13. Lang, J.-W.; Kong, L.-B.; Wu, W.-J.; Liu, M.; Luo, Y.-C.; Kang, L. A Facile Approach to the Preparation of Loose-Packed $Ni(OH)_2$ Nanoflake Materials for Electrochemical Capacitors. *J. Solid State Electrochem.* **2008**, *13*, 333–340.

14. Bastakoti, B. P.; Huang, H.-S.; Chen, L.-C.; Wu, K. C. W.; Yamauchi, Y. Block Copolymer Assisted Synthesis of Porous α-$Ni(OH)_2$ Microflowers with High Surface Areas as Electrochemical Pseudocapacitor Materials. *Chem. Commun.* **2012**, *48*, 9150–9152.
15. Tang, Z.; Tang, C.-h.; Gong, H. A High Energy Density Asymmetric Supercapacitor from Nano-Architectured $Ni(OH)_2$/Carbon Nanotube Electrodes. *Adv. Funct. Mater.* **2012**, *22*, 1272–1278.
16. Zhang, L. L.; Xiong, Z.; Zhao, X. S. A Composite Electrode Consisting of Nickel Hydroxide, Carbon Nanotubes, and Reduced Graphene Oxide with an Ultrahigh Electrocapacitance. *J. Power Sources* **2013**, *222*, 326–332.
17. Park, J. H.; Park, O. O.; Shin, K. H.; Jin, C. S.; Kim, J. H. An Electrochemical Capacitor Based on a $Ni(OH)_2$/Activated Carbon Composite Electrode. *Electrochem. Solid-State Lett.* **2002**, *5*, H7–H10.
18. Huang, Q.; Wang, X.; Li, J.; Dai, C.; Gamboa, S.; Sebastian, P. J. Nickel Hydroxide/Activated Carbon Composite Electrodes for Electrochemical Capacitors. *J. Power Sources* **2007**, *164*, 425–429.
19. Yang, S.; Wu, X.; Chen, C.; Dong, H.; Hu, W.; Wang, X. Spherical α-$Ni(OH)_2$ Nanoarchitecture Grown on Graphene as Advanced Electrochemical Pseudocapacitor Materials. *Chem. Commun.* **2012**, *48*, 2773–2775.
20. Yan, J.; Fan, Z.; Sun, W.; Ning, G.; Wei, T.; Zhang, Q.; Zhang, R.; Zhi, L.; Wei, F. Advanced Asymmetric Supercapacitors Based on $Ni(OH)_2$/Graphene and Porous Graphene Electrodes with High Energy Density. *Adv. Funct. Mater.* **2012**, *22*, 2632–2641.
21. Wang, H.; Liang, Y.; Mirfakhrai, T.; Chen, Z.; Casalongue, H. S.; Dai, H. Advanced Asymmetrical Supercapacitors Based on Graphene Hybrid Materials. *Nano Res.* **2011**, *4*, 729–736.
22. Yang, G.-W.; Xu, C.-L.; Li, H.-L. Electrodeposited Nickel Hydroxide on Nickel Foam with Ultrahigh Capacitance. *Chem. Commun.* **2008**, *44*, 6537–6539.
23. Xiao, T.; Hu, X.; Heng, B.; Chen, X.; Huang, W.; Tao, W.; Wang, H.; Tang, Y.; Tan, X.; Huang, X. $Ni(OH)_2$ Nanosheets Grown on Graphene-Coated Nickel Foam for High-Performance Pseudocapacitors. *J. Alloys Compd.* **2013**, *549*, 147–151.
24. Cao, X.; Shi, Y.; Shi, W.; Lu, G.; Huang, X.; Yan, Q.; Zhang, Q.; Zhang, H. Preparation of Novel 3D Graphene Networks for Supercapacitor Applications. *Small* **2011**, *7*, 3163–3168.
25. Wang, X.; Wang, Y.; Zhao, C.; Zhao, Y.; Yan, B.; Zheng, W. Electrodeposited $Ni(OH)_2$ Nanoflakes on Graphite Nanosheets Prepared by Plasma-Enhanced Chemical Vapor Deposition for Supercapacitor Electrode. *New J. Chem.* **2012**, *36*, 1902–1906.
26. Chen, Z.; Ren, W.; Gao, L.; Liu, B.; Pei, S.; Cheng, H.-M. Three-Dimensional Flexible and Conductive Interconnected Graphene Networks Grown by Chemical Vapour Deposition. *Nat. Mater.* **2011**, *10*, 424–428.
27. Ji, H.; Zhang, L.; Pettes, M. T.; Li, H.; Chen, S.; Shi, L.; Piner, R.; Ruoff, R. S. Ultrathin Graphite Foam: A Three-Dimensional Conductive Network for Battery Electrodes. *Nano Lett.* **2012**, *12*, 2446–2451.
28. Duan, G.; Cai, W.; Luo, Y.; Sun, F. A Hierarchically Structured $Ni(OH)_2$ Monolayer Hollow-Sphere Array and Its Tunable Optical Properties Over a Large Region. *Adv. Funct. Mater.* **2007**, *17*, 644–650.
29. Zhu, L.-P.; Liao, G.-H.; Yang, Y.; Xiao, H.-M.; Wang, J.-F.; Fu, S.-Y. Self-Assembled 3D Flower-Like Hierarchical β-$Ni(OH)_2$ Hollow Architectures and Their *In Situ* Thermal Conversion to NiO. *Nanoscale Res. Lett.* **2009**, *4*, 550–557.
30. Lee, J. W.; Ahn, T.; Kim, J. H.; Ko, J. M.; Kim, J.-D. Nanosheets Based Mesoporous NiO Microspherical Structures *via* Facile and Template-Free Method for High Performance Supercapacitors. *Electrochim. Acta* **2011**, *56*, 4849–4857.
31. Yuan, C.; Zhang, X.; Su, L.; Gao, B.; Shen, L. Facile Synthesis and Self-Assembly of Hierarchical Porous NiO Nano/Micro Spherical Superstructures for High Performance Supercapacitors. *J. Mater. Chem.* **2009**, *19*, 5772–5777.
32. Wang, D. B.; Song, C. X.; Hu, Z. S.; Fu, X. Fabrication of Hollow Spheres and Thin Films of Nickel Hydroxide and Nickel Oxide with Hierarchical Structures. *J. Phys. Chem. B* **2005**, *109*, 1125–1129.
33. Patil, U. M.; Gurav, K. V.; Fulari, V. J.; Lokhande, C. D.; Joo, O. S. Characterization of Honeycomb-Like "β-$Ni(OH)_2$" Thin Films Synthesized by Chemical Bath Deposition Method and Their Supercapacitor Application. *J. Power Sources* **2009**, *188*, 338–342.
34. Corrigan, D. A.; Bendert, R. M. Effect of Coprecipitated Metal Ions on the Electrochemistry of Nickel Hydroxide Thin Films: Cyclic Voltammetry in 1M KOH. *J. Electrochem. Soc.* **1989**, *136*, 723–728.
35. Cai, F.-S.; Zhang, G.-Y.; Chen, J.; Gou, X.-L.; Liu, H.-K.; Dou, S.-X. $Ni(OH)_2$ Tubes with Mesoscale Dimensions as Positive-Electrode Materials of Alkaline Rechargeable Batteries. *Angew. Chem., Int. Ed.* **2004**, *43*, 4212–4216.
36. Wu, Q. D.; Gao, X. P.; Li, G. R.; Pan, G. L.; Yan, T. Y.; Zhu, H. Y. Microstructure and Electrochemical Properties of Al-Substituted Nickel Hydroxides Modified with CoOOH Nanoparticles. *J. Phys. Chem. C* **2007**, *111*, 17082–17087.
37. Murali, S.; Quarles, N.; Zhang, L. L.; Potts, J. R.; Tan, Z.; Lu, Y.; Zhu, Y.; Ruoff, R. S. Volumetric Capacitance of Compressed Activated Microwave-Expanded Graphite Oxide (a-MEGO) Electrodes. *Nano Energy* **2013**, 10.1016/j.nanoen.2013.01.007.
38. Skinner, B.; Chen, T.; Loth, M. S.; Shklovskii, B. I. Theory of Volumetric Capacitance of an Electric Double-Layer Supercapacitor. *Phys. Rev. E* **2011**, *83*, 056102.
39. Zhu, Y.; Murali, S.; Stoller, M. D.; Ganesh, K. J.; Cai, W.; Ferreira, P. J.; Pirkle, A.; Wallace, R. M.; Cychosz, K. A.; Thommes, M.; *et al.* Carbon-Based Supercapacitors Produced by Activation of Graphene. *Science* **2011**, *332*, 1537–1541.
40. Lang, J.-W.; Kong, L.-B.; Liu, M.; Luo, Y.-C.; Kang, L. Asymmetric Supercapacitors Based on Stabilized α-$Ni(OH)_2$ and Activated Carbon. *J. Solid State Electrochem.* **2009**, *14*, 1533–1539.
41. Long, J. W.; Bélanger, D.; Brousse, T.; Sugimoto, W.; Sassin, M. B.; Crosnier, O. Asymmetric Electrochemical Capacitors-Stretching The Limits of Aqueous Electrolytes. *MRS Bull.* **2011**, *36*, 513–522.